ATLAS NOTE

ATLAS-CONF-2011-116

August 19, 2011

Luminosity Determination in pp Collisions at $\sqrt{s} = 7$ TeV using the ATLAS Detector in 2011

The ATLAS Collaboration

Abstract

The luminosity calibration for the ATLAS detector at the LHC during pp collisions at $\sqrt{s} = 7$ TeV in 2011 is presented. Evaluation of the luminosity scale is performed using several luminosity-sensitive detectors, and comparisons of the long-term stability and accuracy of this calibration applied to the 2011 data are made. A relative luminosity uncertainty of $\delta\mathcal{L}/\mathcal{L} = \pm 3.7\%$ is obtained.

1 Introduction

An accurate measurement of the delivered luminosity is a key component of the ATLAS [1] physics program. For cross-section measurements of Standard Model processes the uncertainty on the delivered luminosity is often one of the dominant systematic uncertainties. Searches (and eventual discoveries) of new physics, however, also rely on accurate information about the delivered luminosity to evaluate background levels and determine sensitivity to new physics signatures.

This note describes the preliminary estimate of the ATLAS luminosity for the 2011 pp run at a center-of-mass energy of $\sqrt{s} = 7$ TeV. This analysis is an evolution of the process documented in the initial luminosity paper [2] and updated in the winter 2011 luminosity note [3].

The general method for calibrating the ATLAS luminosity scale remains based on dedicated *van der Meer (vdM)* scans (sometimes also called *beam-separation* or *luminosity* scans) [4]. Due to a number of changes to the ATLAS luminosity detectors during the winter 2011 shutdown, the luminosity calibrations performed in 2010 are not directly applicable to the 2011 data.

Results from a new set of *vdM* scan data taken in May 2011 are described in Section 2. A discussion of the determination of the LHC bunch currents for the May scan is outlined in Section 3. The ATLAS length scale determination for this scan is described in Section 4. A summary of the systematic uncertainties on the luminosity calibration is presented in Section 5 while the calibration results are presented in Section 6. Additional calorimeter-based methods used to evaluate the long-term stability of the luminosity calibration for the 2011 data sample are described in Section 7, and all uncertainties related to the extrapolation of the *vdM* calibration to the full 2011 data sample are detailed in Section 8. The final results and uncertainties are summarized in Section 9.

2 Luminosity Calibration in 2011

2.1 Absolute Luminosity Calibration

The luminosity of a pp collider can be expressed as

$$\mathcal{L} = \frac{\mu n_{\mathrm{b}} f_{\mathrm{r}}}{\sigma_{\mathrm{inel}}} \tag{1}$$

where μ is the average number of inelastic interactions per bunch crossing, n_{b} is the number of colliding bunch pairs, f_{r} is the machine revolution frequency, and σ_{inel} is the pp inelastic cross-section.

As discussed below, ATLAS monitors the delivered luminosity by measuring the observed interaction rate per crossing μ_{vis} independently with a variety of detectors and using several different algorithms. The total luminosity can then be written as

$$\mathcal{L} = \frac{\mu_{\mathrm{vis}} n_{\mathrm{b}} f_{\mathrm{r}}}{\sigma_{\mathrm{vis}}} \tag{2}$$

where $\sigma_{\mathrm{vis}} = \varepsilon \sigma_{\mathrm{inel}}$ is the total inelastic cross-section multiplied by the efficiency ε of a particular detector and algorithm. Since μ_{vis} is an experimentally observable quantity, the calibration of the luminosity scale for a particular detector and algorithm is equivalent to determining the visible cross-section σ_{vis}.

As described in detail in Reference [2], the calibration of σ_{vis} is performed using dedicated *vdM* scans where the absolute luminosity can be inferred from direct measurements of machine parameters. The delivered luminosity can be written as

$$\mathcal{L} = \frac{n_{\mathrm{b}} f_{\mathrm{r}} n_1 n_2}{2\pi \Sigma_x \Sigma_y} \tag{3}$$

where n_1 and n_2 are the bunch populations (protons per bunch) in beam 1 and beam 2 respectively (together forming the bunch charge product), and Σ_x and Σ_y characterize the horizontal and vertical

profiles of the colliding beams. In a *vdM* scan, the beams are separated by steps of a known distance which allows a direct measurement of Σ_x and Σ_y. Combining this with an external measurement of the bunch charge product $n_1 n_2$ provides a direct determination of the luminosity when the beams are unseparated. By comparing this peak luminosity to the peak interaction rate $\mu_{\text{vis}}^{\text{MAX}}$ observed by a given detector and algorithm during the *vdM* scan, a determination of σ_{vis} can be made according to

$$\sigma_{\text{vis}} = \mu_{\text{vis}}^{\text{MAX}} \frac{2\pi\Sigma_x\Sigma_y}{n_1 n_2}. \tag{4}$$

One useful quantity, which only depends on the transverse beam sizes and can be extracted from the *vdM* scan data for each luminosity method, is the specific luminosity $\mathcal{L}_{\text{spec}}$ which can be written as

$$\mathcal{L}_{\text{spec}} = \mathcal{L}/(n_{\text{b}} n_1 n_2) = \frac{f_{\text{r}}}{2\pi\Sigma_x\Sigma_y}. \tag{5}$$

Comparing the specific luminosity values measured in the same scan by different detectors and algorithms provides a direct check on the consistency of the *vdM* scan results from these different methods.

2.2 Converting Counting Rates to Absolute Luminosity

ATLAS primarily uses event counting algorithms to measure the luminosity, where a bunch crossing is said to contain an "event" if the criteria for a given algorithm are satisfied. Event counting is equivalent to "zero counting" where the rate of bunch crossings with no interactions are counted. Since in general there can be more than one interaction per bunch crossing, the visible interaction rate μ_{vis} is a linear function of the event rate only when $\mu_{\text{vis}} \ll 1$. As described more fully in Reference [2], there are two main algorithm types currently being used in ATLAS for luminosity determination: EventOR (inclusive counting) and EventAND (coincidence counting).

In an EventOR algorithm, a bunch crossing will be counted if the sum of all hits on both the forward ("A") and backward ("C") arms of the detector under consideration is at least one. Assuming that the number of interactions in a bunch crossing can be described by a Poisson distribution, the probability of observing an inclusive event can be computed as

$$\begin{aligned} P_{\text{Event\_OR}}(\mu_{\text{vis}}^{\text{OR}}) &= \frac{N_{\text{OR}}}{N_{\text{BC}}} \\ &= 1 - e^{-\mu_{\text{vis}}^{\text{OR}}}. \end{aligned} \tag{6}$$

Here the raw event count N_{OR} is the number of bunch crossings, during a given time, in which at least one pp interaction satisfies the event-selection criteria of the OR algorithm under consideration, and N_{BC} is the total number of bunch crossings during the same interval. Solving for μ_{vis} in terms of the event-counting rate yields:

$$\mu_{\text{vis}}^{\text{OR}} = -\ln\left(1 - \frac{N_{\text{OR}}}{N_{\text{BC}}}\right). \tag{7}$$

In the case of an EventAND algorithm, a bunch crossing will be counted if there is at least one hit on both sides of the detector. The probability of recording a coincidence event can be expressed as

$$\begin{aligned} P_{\text{Event\_AND}}(\mu_{\text{vis}}^{\text{AND}}) &= \frac{N_{\text{AND}}}{N_{\text{BC}}} \\ &= 1 - 2e^{-(1+\sigma_{\text{vis}}^{\text{OR}}/\sigma_{\text{vis}}^{\text{AND}})\mu_{\text{vis}}^{\text{AND}}/2} + e^{-(\sigma_{\text{vis}}^{\text{OR}}/\sigma_{\text{vis}}^{\text{AND}})\mu_{\text{vis}}^{\text{AND}}}. \end{aligned} \tag{8}$$

This relationship cannot be inverted analytically to determine $\mu_{\text{vis}}^{\text{AND}}$ as a function of $N_{\text{AND}}/N_{\text{BC}}$ so some other technique must be used. Typically this inversion is performed numerically using a look-up table, or the function is inverted for a specific value of μ using an iterative technique, such as the Newton-Raphson method.

	vdM Scan IV–V (1 October, 2010)	*vdM* Scan VII–VIII (15 May, 2011)
LHC Fill Number	1386	1783
Scan Directions	2 sets of horizontal plus vertical scans	
Total Scan Steps per Plane	25 ($\pm 6\sigma_b$)	25 ($\pm 6\sigma_b$)
Scan Duration per Step	20 s	20 s
Number of bunches colliding in ATLAS & CMS	6	14
Total number of bunches per beam	19	38
Number of protons per bunch	$\sim 0.9 \cdot 10^{11}$	$\sim 0.8 \cdot 10^{11}$
β-function at IP [$\beta^\star$] (m)	~ 3.5	~ 1.5
Transverse single beam size σ_b (μm)	~ 60	~ 40
Half crossing angle (μrad)	± 100	± 120
Typical luminosity/bunch ($\mu b^{-1}/s$)	0.22	0.38
μ (interactions/crossing)	1.3	2.3

Table 1: Summary of the main characteristics of the 2011 *vdM* scans performed at the ATLAS interaction point compared to the final scans performed in 2010. The values of luminosity/bunch and μ are given for zero beam separation.

2.3 Luminosity-Scan Data

The beam conditions during the dedicated *vdM* scans are different from those in normal physics operations, with fewer bunches colliding, no bunch trains, and lower bunch intensities. These conditions are chosen to reduce various systematic uncertainties in the scan procedure.

As discussed in Section 8, there were a number of changes to the ATLAS detector during the 2010-11 winter shutdown and during the initial 2011 LHC running which made it difficult to apply the 2010 luminosity calibration directly to the 2011 data. As a result, the 2011 calibration relies on a pair of *vdM* scans which were taken on 15 May, 2011. As shown in Table 1, these May 2011 scans (numbered VII and VIII) were performed with a relatively large number of bunches ($n_b = 14$) in the machine compared to the final 2010 scans, and had a slightly larger peak luminosity per bunch, with $\mu \approx 2.3$.

Each colliding bunch pair can be identified numerically by its Bunch-Crossing Identifier number (BCID) which labels each of the 3564 possible 25 ns slots in the nominal LHC fill pattern. Since the luminosity can be different for each colliding bunch pair, both because the beam sizes can vary bunch-to-bunch but also because the bunch charge product $n_1 n_2$ can vary at the level of 10-20%, the determination of $\Sigma_{x/y}$ and the measurement of $\mu_{\rm vis}^{\rm MAX}$ must be performed independently for each BCID.

As a result, the May 2011 scan provides 14 independent measurements of $\sigma_{\rm vis}$ within the same scan, providing additional consistency checks for the calibration procedure. The filling pattern used had a minimum separation between collisions of 50 BCIDs, or a time of $1.25\,\mu s$. Two sets of scans, each consisting of one horizontal and one vertical scan, were performed in short succession so as to quantify the reproducibility of the optimal relative beam position, convolved beam sizes, and visible cross-sections.

2.4 Luminosity Detectors

There are two primary detectors used to make bunch-by-bunch luminosity measurements: LUCID and BCM.

LUCID is a Cerenkov detector specifically designed for measuring the luminosity in ATLAS. Sixteen mechanically polished aluminum tubes filled with C_4F_{10} gas surround the beampipe on each side of the

interaction point (IP) at a distance of 17 m, covering the pseudorapidity range $5.6 < |\eta| < 6.0$. The Cerenkov photons created by charged particles in the gas are reflected by the tube walls until they reach photomultipliers (PMT) situated at the back end of the tubes. If one of the LUCID PMTs produces a signal over a preset threshold, that tube records a "hit" for that event. The LUCID detector electronics receive signals from the LHC clock allowing it to record event rates separately for each BCID.

The Beam Conditions Monitor (BCM) consists of four small diamond sensors on each side of the ATLAS IP arranged around the beampipe in a cross pattern. The BCM is a fast device primarily designed to monitor background levels and issue a beam-abort request in case beam losses start to risk damage to ATLAS detectors. The fast readout of the BCM also provides a useful, low acceptance bunch-by-bunch luminosity signal at $|\eta| = 4.2$. The horizontal and vertical pairs of BCM detectors are read out separately, leading to two luminosity measurements labelled BCMH and BCMV respectively. Because the acceptance, thresholds, and data path may all have small differences between BCMH and BCMV, these two measurements are treated as being made by independent devices for calibration and monitoring purposes, although the overall response of the two devices is expected to be very similar. The BCMH readout was previously available for luminosity measurements in 2010, while the BCMV readout has only been considered in 2011.

2.5 Scan Analysis for Fill 1783

The two May 2011 *vdM* scans have been used to derive calibrations for the LUCID and BCM detectors. The data from each detector is analysed according to several different algorithms, notably the inclusive EventOR algorithm and the coincidence EventAND algorithm.

In addition to the LUCID_EventOR and LUCID_EventAND algorithms, there are two additional LUCID algorithms which just consider at least one hit above threshold on the A and C side separately. Events passing these LUCID_EventA and LUCID_EventC algorithms are clearly subsets of the events passing the LUCID_EventOR algorithm, and these single-sided algorithms have been mostly used to monitor the stability of the LUCID detector. Since there are two independent BCM readouts (BCMH and BCMV) there are a total of four BCM algorithms calibrated in the May scan.

For each individual algorithm, the *vdM* scan data are analysed in a very similar manner. For each BCID, the specific visible interaction rate $\mu_{\rm vis}/(n_1 n_2)$ is plotted *vs.* the "nominal" beam separation, *i.e.* the separation specified by the LHC control system for each scan step. The specific interaction rate is used so that the result is not affected by the change in beam currents over the duration of the scan. An example of the *vdM* scan data for a single BCID from scan VII in the x plane is shown in Figure 1.

The value of $\mu_{\rm vis}$ is determined from the raw event rate using the analytic function described in Section 2.2 for the inclusive EventOR algorithms. The coincidence EventAND algorithms are more involved, and a numerical inversion is performed to determine $\mu_{\rm vis}$ from the raw EventAND rate. Since the EventAND μ determination depends on $\sigma_{\rm vis}^{\rm AND}$ as well as $\sigma_{\rm vis}^{\rm OR}$, an iterative procedure must be employed. This procedure is found to converge after a few steps.

Each scan for each BCID is fit independently to a Gaussian function plus constant background to provide a measurement of $\mu_{\rm vis}^{\rm MAX}$ and Σ. Previous scans had used double Gaussian fits, but for the May 2011 scan data this was found to be unnecessary. For the BCM_EventAND algorithms, the background level is found to be consistent with zero, and just a single Gaussian function has been used.

The combination of one x scan and one y scan is the minimum needed to perform a measurement of $\sigma_{\rm vis}$. The average value of $\mu_{\rm vis}^{\rm MAX}$ between the two scan planes is used in the determination of $\sigma_{\rm vis}$, and the correlation matrix from each fit between $\mu_{\rm vis}^{\rm MAX}$ and Σ is taken into account when evaluating the statistical uncertainty.

Tables 2 through 5 summarize the scan VII-VIII measurements of $\sigma_{\rm vis}$ for the eight different LUCID and BCM algorithms. Since $\sigma_{\rm vis}$ should be independent of BCID or scan number, the agreement between

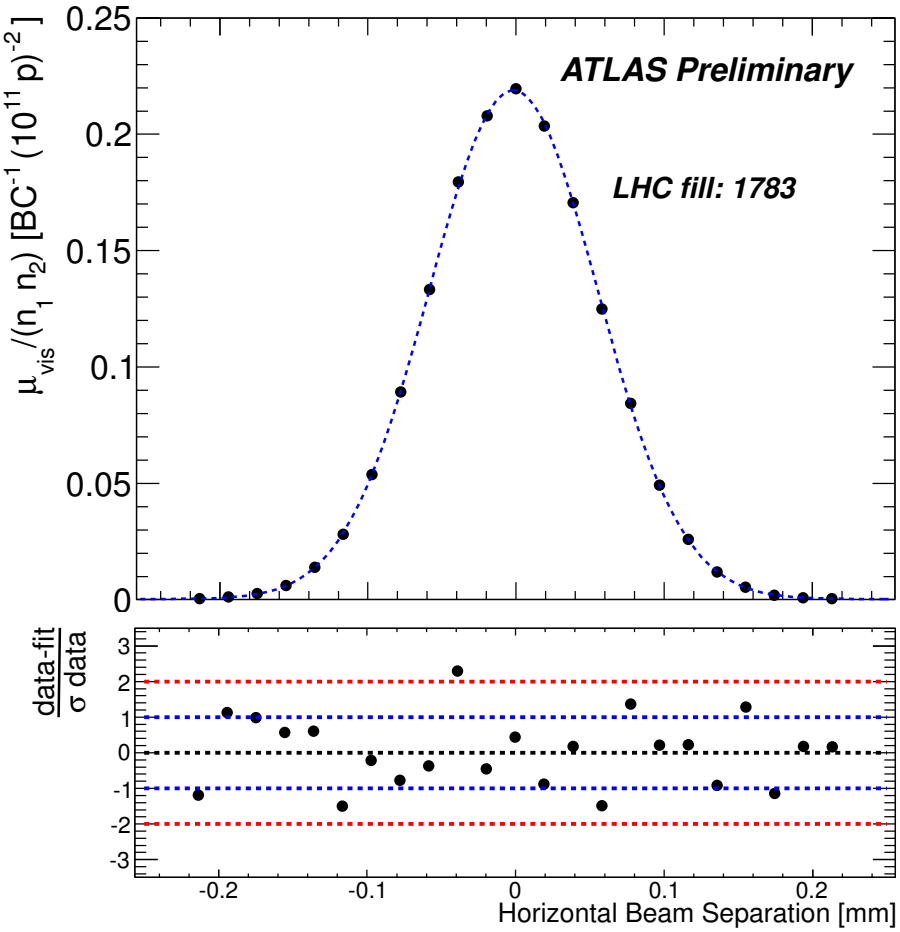

Figure 1: Specific interaction rate versus nominal beam separation for the BCMH_EventOR algorithm during scan VII in the x plane for BCID 817. The residual deviation of the data from the Gaussian plus constant background fit assuming statistical errors only is shown in the bottom panel.

these values for a given algorithm reflects the reproducibility and stability of the calibration procedure during a single fill.

Figure 2 shows the σ_{vis} values determined for LUCID_EventOR separately by BCID and by scan. The RMS variation seen between the σ_{vis} results measured for different BCIDs is 0.4% for scan VII and 0.3% for scan VIII. The BCID-averaged σ_{vis} values found in scans VII and VIII agree to 0.4% for all four LUCID algorithms. Similar data for the BCMH_EventOR algorithm are shown in Figure 3. Again an RMS variation between BCIDs of up to 0.4% is seen, and a difference between the two scans of 0.4% is observed for both BCM_EventOR algorithms. The agreement in the BCM_EventAND algorithms is worse, with an RMS around 1%, although these measurements also have significantly larger statistical errors.

	LUCID_EventOR σ_{vis} (mb)		LUCID_EventAND σ_{vis} (mb)	
BCID	Scan VII	Scan VIII	Scan VII	Scan VIII
81	42.52 ± 0.04	42.73 ± 0.04	13.49 ± 0.02	13.49 ± 0.02
131	42.27 ± 0.04	42.42 ± 0.04	13.34 ± 0.01	13.47 ± 0.01
181	42.18 ± 0.04	42.34 ± 0.04	13.32 ± 0.01	13.40 ± 0.01
231	42.52 ± 0.04	42.71 ± 0.04	13.42 ± 0.01	13.52 ± 0.01
281	42.66 ± 0.04	42.75 ± 0.04	13.47 ± 0.01	13.53 ± 0.01
331	42.50 ± 0.04	42.73 ± 0.04	13.44 ± 0.01	13.52 ± 0.01
817	42.52 ± 0.04	42.61 ± 0.04	13.43 ± 0.01	13.48 ± 0.01
867	42.62 ± 0.04	42.65 ± 0.04	13.47 ± 0.01	13.48 ± 0.01
917	42.55 ± 0.04	42.61 ± 0.04	13.47 ± 0.01	13.46 ± 0.01
967	42.57 ± 0.04	42.63 ± 0.04	13.47 ± 0.01	13.47 ± 0.01
2602	42.37 ± 0.04	42.55 ± 0.04	13.39 ± 0.01	13.45 ± 0.01
2652	42.26 ± 0.04	42.43 ± 0.04	13.38 ± 0.01	13.42 ± 0.01
2702	42.25 ± 0.04	42.49 ± 0.04	13.34 ± 0.01	13.43 ± 0.01
2752	42.30 ± 0.04	42.58 ± 0.04	13.38 ± 0.01	13.44 ± 0.01
Average	42.43 ± 0.01	42.59 ± 0.01	13.41 ± 0.00	13.47 ± 0.00
RMS	0.36%	0.29%	0.41%	0.27%

Table 2: Measured σ_{vis} values for LUCID_EventOR and LUCID_EventAND algorithms by BCID. Errors shown are statistical only.

2.6 Internal Scan Consistency

The variation between the measured σ_{vis} values by BCID and between scans demonstrates the stability and reproducibility of the calibration technique. Comparing Figures 2 and 3 it is clear that some of the variation seen in σ_{vis} is not statistical in nature, but rather is correlated by BCID. As discussed in Section 5, the RMS variation of σ_{vis} between BCIDs within a given scan is taken as a systematic uncertainty in the calibration technique, as is the reproducibility of σ_{vis} between scans. The yellow band in these figures, which represents a range of ±0.6%, shows the quadrature sum of these two systematic uncertainties, which are discussed further in Section 5.

Further checks can be made by considering the distribution of $\mathcal{L}_{\text{spec}}$ defined in Equation 5 for a given BCID as measured by different algorithms. Since this quantity depends only on the convolved beam sizes, consistent results should be measured by all methods. Figure 4 shows the measured $\mathcal{L}_{\text{spec}}$ values by BCID and scan for LUCID and BCMH algorithms, as well as the ratio of these values. Bunch-to-bunch variations of the specific luminosity are typically 5–10%, reflecting bunch-to-bunch differences in transverse emittance typical of routine physics operations. For each BCID, however, all algorithms are

	LUCID_EventA σ_{vis} (mb)		LUCID_EventC σ_{vis} (mb)	
BCID	Scan VII	Scan VIII	Scan VII	Scan VIII
81	27.99 ± 0.03	28.09 ± 0.03	28.05 ± 0.03	28.16 ± 0.03
131	27.76 ± 0.03	27.91 ± 0.03	27.83 ± 0.03	27.98 ± 0.03
181	27.72 ± 0.03	27.83 ± 0.03	27.77 ± 0.03	27.90 ± 0.03
231	27.94 ± 0.03	28.09 ± 0.03	28.01 ± 0.03	28.17 ± 0.03
281	28.05 ± 0.03	28.12 ± 0.03	28.10 ± 0.03	28.19 ± 0.03
331	27.98 ± 0.03	28.10 ± 0.03	27.96 ± 0.03	28.16 ± 0.03
817	27.96 ± 0.03	28.02 ± 0.03	28.00 ± 0.03	28.07 ± 0.03
867	28.02 ± 0.03	28.05 ± 0.03	28.09 ± 0.03	28.09 ± 0.03
917	28.00 ± 0.03	28.03 ± 0.03	28.03 ± 0.03	28.05 ± 0.03
967	27.98 ± 0.03	28.01 ± 0.03	28.05 ± 0.03	28.10 ± 0.03
2602	27.83 ± 0.03	27.95 ± 0.03	27.91 ± 0.03	28.04 ± 0.03
2652	27.79 ± 0.03	27.89 ± 0.03	27.85 ± 0.03	27.95 ± 0.03
2702	27.76 ± 0.03	27.89 ± 0.03	27.79 ± 0.03	28.00 ± 0.03
2752	27.79 ± 0.03	27.99 ± 0.03	27.87 ± 0.03	28.01 ± 0.03
Average	27.90 ± 0.01	28.00 ± 0.01	27.95 ± 0.01	28.06 ± 0.01
RMS	0.40%	0.31%	0.39%	0.30%

Table 3: Measured σ_{vis} values for LUCID_EventA and LUCID_EventC algorithms by BCID. Errors shown are statistical only.

	BCMH_EventOR σ_{vis} (mb)		BCMH_EventAND σ_{vis} (mb)	
BCID	Scan VII	Scan VIII	Scan VII	Scan VIII
81	4.690 ± 0.010	4.728 ± 0.010	0.1342 ± 0.0011	0.1378 ± 0.0012
131	4.667 ± 0.009	4.681 ± 0.010	0.1312 ± 0.0010	0.1368 ± 0.0010
181	4.642 ± 0.010	4.685 ± 0.010	0.1354 ± 0.0010	0.1357 ± 0.0011
231	4.686 ± 0.009	4.720 ± 0.009	0.1376 ± 0.0010	0.1382 ± 0.0010
281	4.685 ± 0.009	4.710 ± 0.010	0.1377 ± 0.0010	0.1354 ± 0.0010
331	4.694 ± 0.009	4.702 ± 0.010	0.1362 ± 0.0011	0.1343 ± 0.0011
817	4.696 ± 0.009	4.711 ± 0.009	0.1368 ± 0.0010	0.1383 ± 0.0010
867	4.694 ± 0.009	4.697 ± 0.009	0.1351 ± 0.0010	0.1367 ± 0.0010
917	4.706 ± 0.009	4.695 ± 0.010	0.1374 ± 0.0010	0.1385 ± 0.0011
967	4.697 ± 0.009	4.710 ± 0.009	0.1357 ± 0.0009	0.1371 ± 0.0009
2602	4.673 ± 0.009	4.688 ± 0.009	0.1358 ± 0.0009	0.1372 ± 0.0009
2652	4.653 ± 0.009	4.681 ± 0.010	0.1333 ± 0.0010	0.1356 ± 0.0010
2702	4.663 ± 0.009	4.683 ± 0.009	0.1359 ± 0.0010	0.1358 ± 0.0010
2752	4.655 ± 0.009	4.702 ± 0.009	0.1334 ± 0.0010	0.1341 ± 0.0010
Average	4.679 ± 0.002	4.699 ± 0.003	0.1354 ± 0.0003	0.1365 ± 0.0003
RMS	0.41%	0.31%	1.3%	1.0%

Table 4: Measured σ_{vis} values for BCMH_EventOR and BCMH_EventAND by BCID. Errors shown are statistical only.

	BCMV_EventOR σ_{vis} (mb)		BCMV_EventAND σ_{vis} (mb)	
BCID	Scan VII	Scan VIII	Scan VII	Scan VIII
81	4.755 ± 0.010	4.763 ± 0.010	0.1391 ± 0.0011	0.1397 ± 0.0012
131	4.700 ± 0.010	4.736 ± 0.010	0.1360 ± 0.0010	0.1379 ± 0.0010
181	4.696 ± 0.010	4.728 ± 0.010	0.1375 ± 0.0011	0.1386 ± 0.0011
231	4.732 ± 0.009	4.751 ± 0.010	0.1373 ± 0.0010	0.1418 ± 0.0010
281	4.746 ± 0.010	4.757 ± 0.010	0.1383 ± 0.0010	0.1383 ± 0.0011
331	4.726 ± 0.010	4.752 ± 0.009	0.1400 ± 0.0011	0.1375 ± 0.0011
817	4.739 ± 0.009	4.746 ± 0.009	0.1392 ± 0.0010	0.1404 ± 0.0010
867	4.739 ± 0.009	4.738 ± 0.009	0.1395 ± 0.0010	0.1393 ± 0.0010
917	4.743 ± 0.010	4.760 ± 0.010	0.1390 ± 0.0010	0.1394 ± 0.0010
967	4.732 ± 0.009	4.742 ± 0.009	0.1393 ± 0.0009	0.1388 ± 0.0009
2602	4.706 ± 0.009	4.759 ± 0.009	0.1379 ± 0.0009	0.1407 ± 0.0009
2652	4.724 ± 0.010	4.735 ± 0.010	0.1377 ± 0.0011	0.1417 ± 0.0011
2702	4.722 ± 0.009	4.749 ± 0.009	0.1402 ± 0.0010	0.1380 ± 0.0010
2752	4.709 ± 0.009	4.742 ± 0.009	0.1360 ± 0.0010	0.1358 ± 0.0010
Average	4.726 ± 0.003	4.747 ± 0.003	0.1383 ± 0.0003	0.1391 ± 0.0003
RMS	0.37%	0.22%	0.9%	1.2%

Table 5: Measured σ_{vis} values for BCMV_EventOR and BCMV_EventAND by BCID. Errors shown are statistical only.

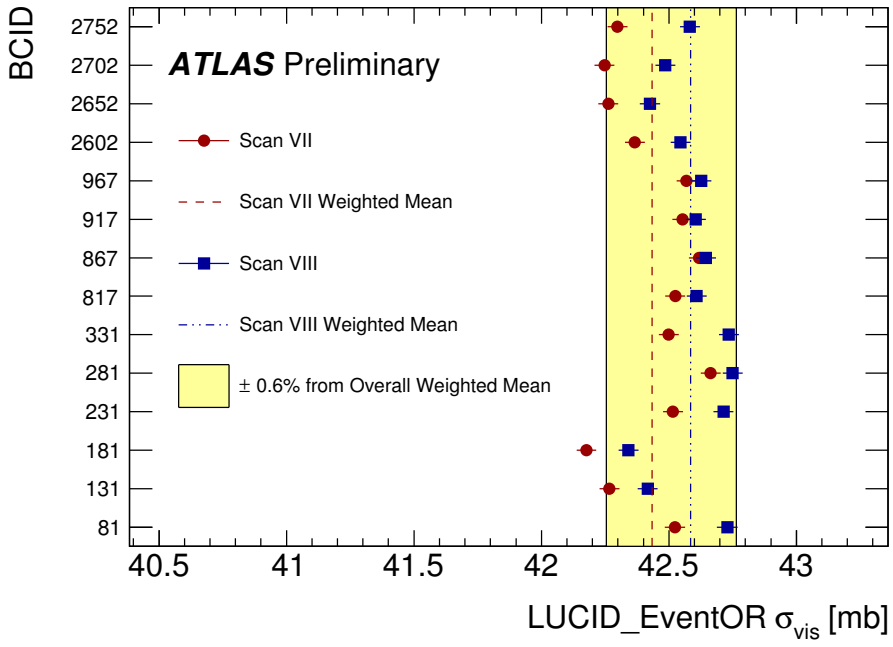

Figure 2: Measured σ_{vis} values for LUCID_EventOR by BCID for scans VII and VIII. The error bars represent statistical errors only. The vertical lines indicate the weighted average over BCIDs for Scans VII and VIII separately. The yellow band indicates a ±0.6% variation from the average, which is the systematic uncertainty evaluated from the per-BCID and per-scan σ_{vis} consistency.

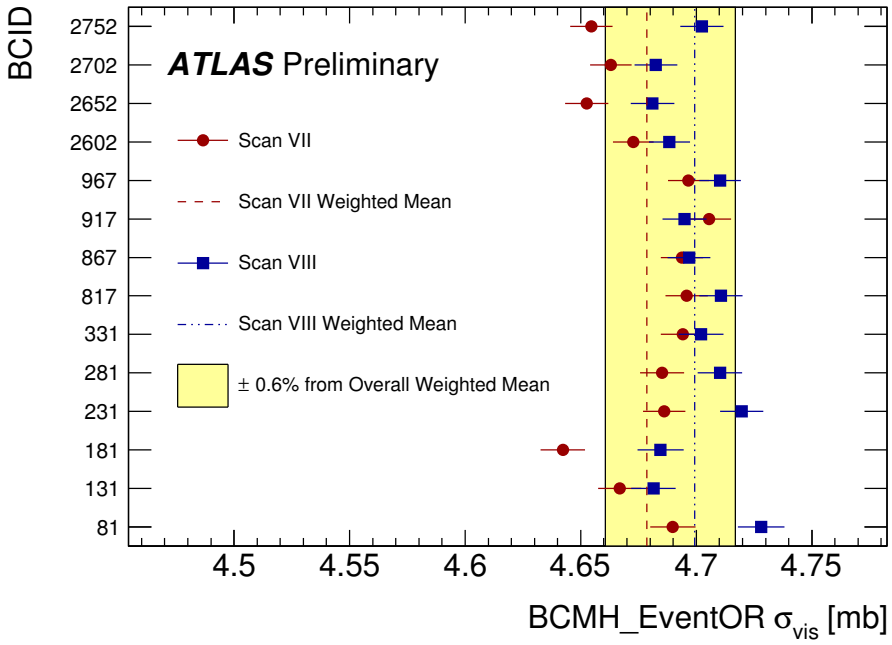

Figure 3: Measured σ_{vis} values for BCMH_EventOR by BCID for scans VII and VIII. The error bars represent statistical errors only. The vertical lines indicate the weighted average over BCIDs for Scans VII and VIII separately. The yellow band indicates a ±0.6% variation from the average, which is the systematic uncertainty evaluated from the per-BCID and per-scan σ_{vis} consistency.

statistically consistent. A small systematic reduction in $\mathcal{L}_{\text{spec}}$ can be observed between scans VII and VIII, which is due to emittance growth in the colliding beams.

Figure 5 shows the Σ_x and Σ_y values determined by the BCM algorithms during scans VII and VIII, and for each BCID a clear increase can be seen with time. This emittance growth can also be seen clearly as a reduction in the peak specific interaction rate $\mu_{\text{vis}}^{\text{MAX}}/(n_1 n_2)$ shown in Figure 6 for BCMH_EventOR. Here the peak rate is shown for each of the four individual horizontal and vertical scans, and a clear monotonic decrease in rate is observed. The fact that the σ_{vis} values are consistent between scan VII and scan VIII demonstrates that to first order the emittance growth factors out of the measured luminosity calibration factors. The residual uncertainty associated with emittance growth is discussed in Section 5.

3 LHC Bunch Currents

The dominant systematic uncertainty on the 2010 luminosity calibration, described in Reference [3], was associated with the determination of the bunch charge product $(n_1 n_2)$ for each colliding BCID. Performing the luminosity calibration on a bunch-by-bunch basis is essential for the reasons described in Section 2.3. Measuring the bunch charge product separately for each BCID is also unavoidable as only a subset of the circulating bunches collide in ATLAS (14 out of 38 during the 2011 scan).

The uncertainty on this bunch charge product was found by the Bunch Current Normalization Working Group (BCNWG) to be 3.1% in scans IV-V taken in October 2010 [5]. A brief summary of that analysis is presented below, along with preliminary updates of the bunch charge uncertainties for the 2011 *vdM* scans.

The bunch currents in the LHC are determined by eight Bunch Current Transformers (BCTs) in a multi-step process due to the different capabilities of the available instrumentation. Each beam is

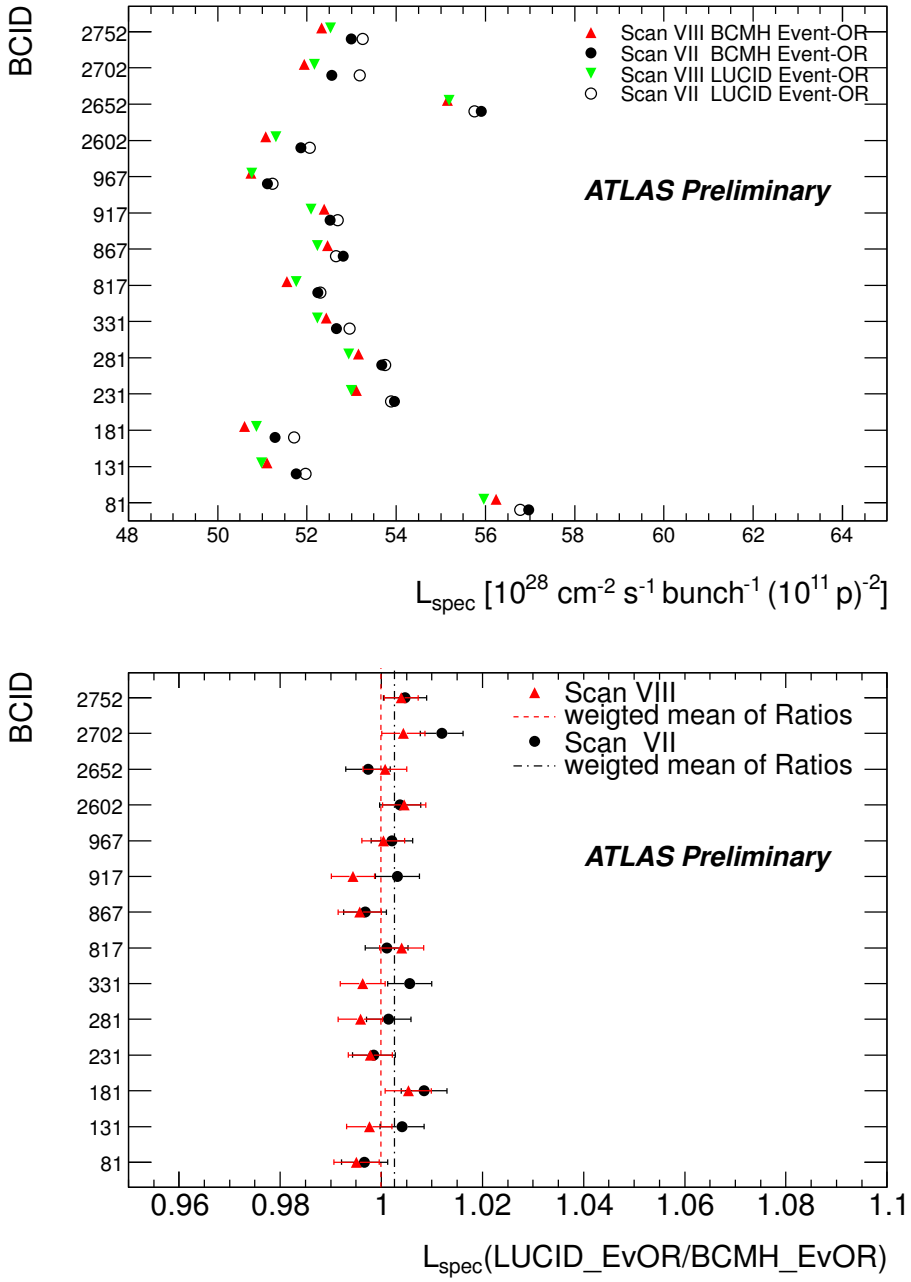

Figure 4: Specific luminosity determined by BCMH and LUCID per BCID for scans VII and VIII. The figure on the top shows the specific luminosity values determined by BCMH_EventOR and LUCID_EventOR, while the figure on the bottom shows the ratios of these values. The vertical lines indicate the weighted average over BCIDs for scans VII and VIII separately. The error bars represent statistical errors only.

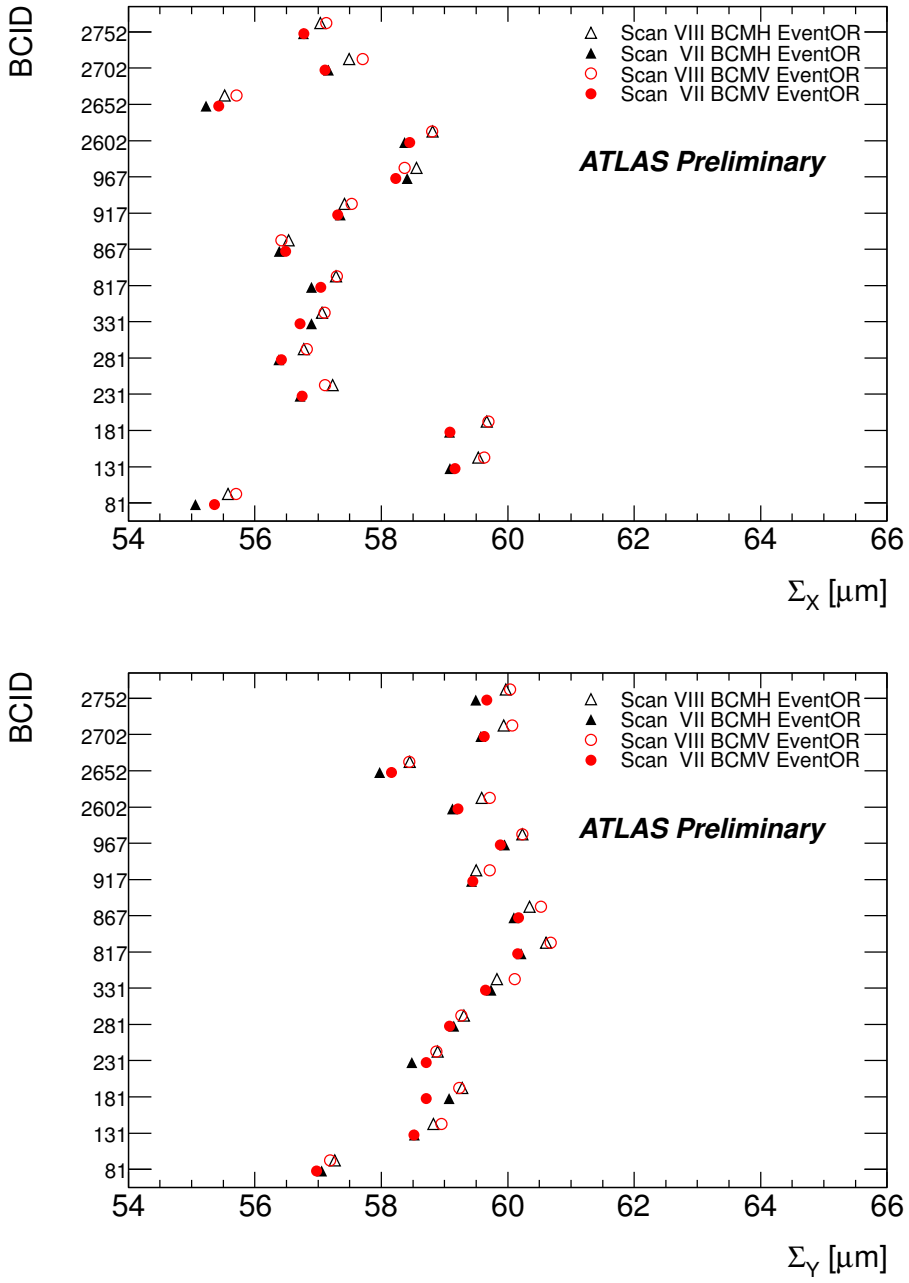

Figure 5: Σ_x (top) and Σ_y (bottom) determined by BCM_EventOR algorithms per BCID for scans VII and VIII. The statistical uncertainty on each measurement is approximately the size of the marker.

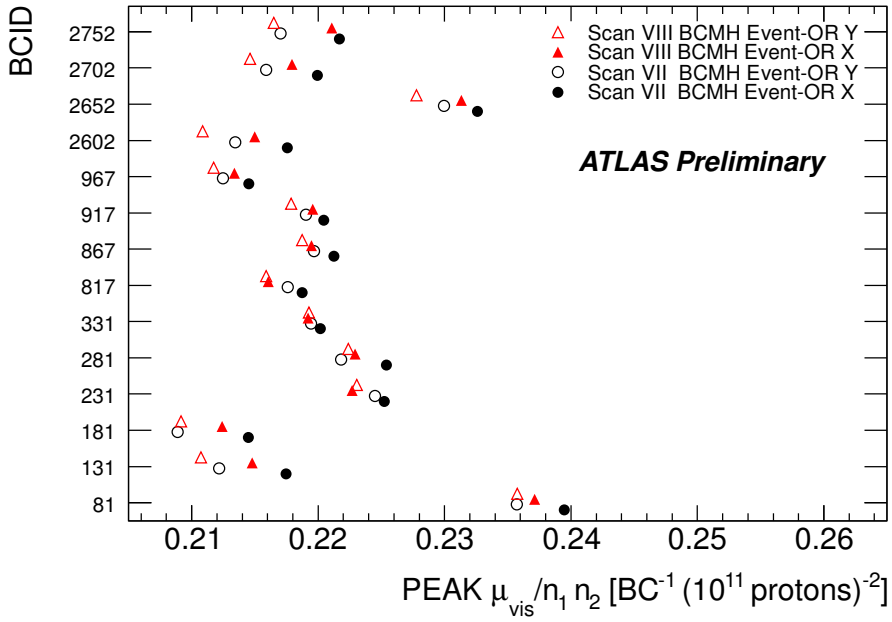

Figure 6: Peak $\mu_{\text{vis}}/(n_1 n_2)$ determined by BCMH_EventOR per BCID for scans VII and VIII. The statistical uncertainty on each measurement is approximately the size of the marker.

monitored by two identical and redundant DC current transformers (DCCT) which are high accuracy devices but do not have any ability to separate individual bunch charges. Each beam is also monitored by two fast beam current transformers (FBCT) which have the ability to measure bunch currents individually for each of the 3564 nominal 25 ns slots in each beam. The relative fraction of the total current in each BCID can be determined from the FBCT system, but this relative measurement must be normalized to the overall current scale provided by the DCCT. Additional corrections are made for any out-of-time charge that may be present in a given BCID but not colliding at the interaction point.

Combining all of these effects together, the bunch charge in BCID i for beam 1 or beam 2 can be determined as

$$n_{1/2}(i) = (N_{\text{tot}}^{\text{DCCT}} - N_{\text{ghost}}) \cdot \frac{S_i^{\text{FBCT}}}{\sum S_i^{\text{FBCT}}} \tag{9}$$

where $N_{\text{tot}}^{\text{DCCT}}$ is the total calibrated charge observed by the DCCT, N_{ghost} is a correction for "ghost charge", and S_i^{FBCT} is the signal observed by the FBCT in BCID i. Ghost charge, discussed further in Section 3, refers to BCIDs filled with less than $\sim 10^8$ protons which are seen by the DCCT but are below the FBCT threshold. The total DCCT charge is further computed as

$$N_{\text{tot}}^{\text{DCCT}} = \alpha \cdot S^{\text{DCCT}} - N_0^{\text{DCCT}} \tag{10}$$

where α is the DCCT scale factor, S^{DCCT} is the signal observed by the DCCT, and N_0^{DCCT} is the DCCT baseline offset correction. The uncertainties on each of these parameters are evaluated separately and discussed below.

DCCT baseline offset

The DCCT is known to have baseline drifts for a variety of reasons including temperature effects, mechanical vibrations, and electromagnetic pick-up in cables. For each fill the baseline readings for each beam (corresponding to zero current) must be determined by looking at periods with

no beam immediately before and after each fill. Due to the possible variation of this baseline correction over a fill, uncertainties have been evaluated based on the observed size of these drifts over time. Because the baseline offsets vary by at most $\pm 0.8 \times 10^9$ protons in each beam, the relative uncertainty from the baseline determination decreases as the total circulating currents go up. With the total currents stored in scans VII-VIII, this represents a small uncertainty ($\pm 0.1\%$).

DCCT scale variation

In addition to the baseline correction, the absolute scale of the DCCT must be understood. The current source used to calibrate the DCCT has a quoted accuracy of 0.1% from the manufacturer, therefore the intrinsic accuracy of the device will contribute a negligible systematic uncertainty compared to other sources. Other systematic uncertainties on the absolute DCCT scale could come from unexpected non-linearities, from a potential dependence on the LHC fill pattern, bunch length or local orbit distortions, and from imperfect long-term reproducibility. The DCCT was calibrated using the precise current source several times in 2010 during technical stops in the LHC program. This DCCT calibration campaign was continued in 2011, but so far the statistics are not adequate to improve the uncertainty from 2010. To quantify possible variations of the DCCT scale with time, the peak-to-peak variation observed in these dedicated DCCT calibrations has been used to estimate an overall scale uncertainty of $\pm 2.7\%$.

Bunch-to-bunch fraction

Since the DCCT can only measure the total bunch charge in each beam, the FBCT is used to determine the relative fraction of bunch charge in each BCID, such that the bunch charge product colliding in a particular BCID can be determined. To evaluate possible errors in the bunch-to-bunch determination a check was made by comparing the FBCT values against the ATLAS beam pick-up timing system, which also can measure the bunch current for an individual BCID. The variation seen between these systems is taken as a systematic uncertainty, and since there was no apparent correlated offset between these results, this uncertainty is assumed to be uncorrelated between beams. The resulting uncertainty on the bunch charge product is $\pm 1.3\%$.

Ghost charge and satellite bunches Another source of uncertainty is the presence of ghost charge and satellite bunches. For a variety of reasons, charge can be captured by either the SPS or LHC RF system outside the proper 2.5 ns RF bucket for collisions at a given IP. All of these charges will contribute to the current measured by the DCCT, and any charge within a given 25 ns slot will also contribute to the relative fraction measured by the FBCT if the total charge in that BCID is above the FBCT sensitivity threshold.

Charge which lies below FBCT threshold has been named ghost charge since it remains invisible to the FBCT, although it is still integrated by the DCCT. The LHC longitudinal-density monitors (LDM) [6] were used to measure the relative proton population in every single RF bucket during LHC fill 1783. The resulting fraction of circulating charge in all but the nominally filled BCIDs was found to be 0.18 (0.40) % in beam 1 (2), albeit with a large fractional uncertainty associated with the details of the pedestal subtraction procedure. An independent determination was provided by the ATLAS BCM, whose excellent timing resolution (2-3 ns) was exploited to measure the fraction of incoming-beam halo in all but the nominally filled BCIDs, relative to the halo associated with the unpaired bunches in each beam (*i.e.* the bunches that do not collide in ATLAS). The resulting ghost charge fractions were 0.07 (0.06) % in beam 1 (2). Averaging the LDM and BCM results yields a total correction of -0.35% on the bunch-current product, that was applied after normalizing the total FBCT charge to that measured by the DCCT.

Satellite bunches refer to charge which is in the wrong 2.5 ns RF bucket close to a normal colliding bunch. This satellite bunch will produce luminosity within a given 25 ns BCID window, but is

offset both in space and time from the nominal IP. Depending upon the crossing angle, the time difference between the satellite and the nominal bunch, and the specifics of the luminosity detector, these satellite collisions may or may not contribute to the signal observed during the *vdM* scan.

The satellite bunch analysis performed for the 2010 *vdM* scans [7] has been repeated on the May 2011 scan. Satellite bunches in ATLAS are detected by extending the tracking and vertexing algorithms to cover a longitudinal distance ±1 m from the nominal interaction point. This distance covers the expected satellite interaction points for bunches displaced by up to ±75 cm which corresponds to a ±5 ns time displacement, or two RF buckets. After applying vertex efficiency corrections as a function of longitudinal distance derived from Monte Carlo simulations, a corrected vertex distribution can be produced, as shown in Figure 7. The small bumps at ±37.5 cm and ±75 cm are evidence for satellite collisions in the May 2011 scan. After corrections for the crossing angle in the $y - z$ plane and the dependence of the transverse beam size on longitudinal position (the hourglass effect), an upper limit on the total satellite bunch charge is determined to be 0.1%.

From the allowed upper limit of both the ghost charge and satellite collisions, a systematic uncertainty on the determination of the bunch charge product of 0.18% is found.

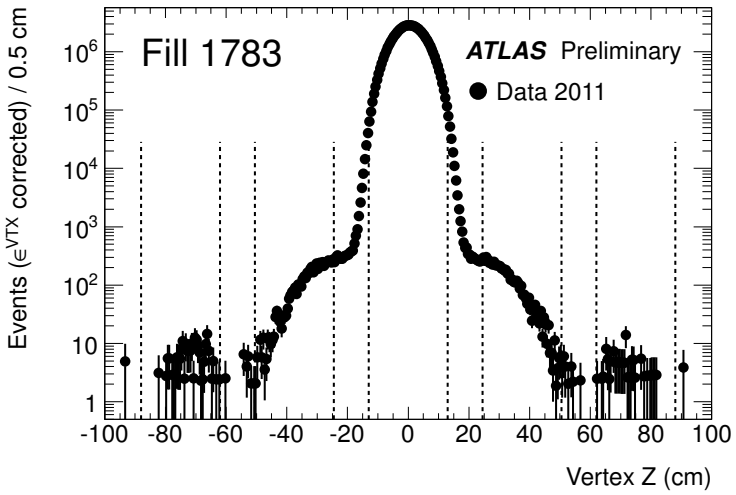

Figure 7: Longitudinal distribution of vertices during May 2011 *vdM* scan, corrected for vertex efficiency.

The relative uncertainty on the bunch charge product ($n_1 n_2$) is shown in Table 6 for the May 2011 *vdM* scan taken in LHC fill 1783. The uncertainty is found to be 3.03%.

Scan Number	VII–VIII
Fill Number	1783
DCCT baseline offset	0.1%
DCCT scale variation	2.7%
Bunch-to-bunch fraction	1.3%
Ghost charge and satellite bunches	0.2%
Total	3.0%

Table 6: Systematic uncertainties on the determination of the bunch charge product $n_1 n_2$ for the May 2011 *vdM* scan fill.

4 Length Scale Calibration

One key input to the *vdM* scan technique is the knowledge about the beam separation at every scan point. The assumption that the absolute luminosity can be derived from the beam profiles using Equation 3 relies directly on this knowledge of the beam separation length scale through the measurement of Σ_x and Σ_y during the scans. The amount of beam displacement is controlled by a set of closed orbit bumps applied locally near the ATLAS IP using steering correctors. To verify this length scale, a dedicated length scale calibration measurement was performed on May 16th 2011[1], where a series of scans were made displacing the beams in collision by five steps over a range of $\pm 120\,\mu$m. Because the beams remain in collision during these scans, the actual position of the luminous region can be reconstructed with high accuracy using the primary vertex position reconstructed by the ATLAS detector.

Since each of the four bump amplitudes (two beams in two transverse directions) depends on different magnet and lattice functions, the distance-scale calibration scans were performed so that each of these four calibration constants could be extracted independently. The results of the four individual calibrations are summarized in Table 7. Because the luminosity-calibration scans discussed in Section 2 were performed by separating the two beams symmetrically in opposite directions, the relevant scale factor in the determination of $\Sigma_{x/y}$ is the average of the scale factors for beam 1 and beam 2 in each plane. The resulting distance scales are seen to be consistent with unity in the horizontal direction at the 0.05% level, and deviating from unity in the vertical direction at the 0.30% level. Since this is a relatively small effect, the length scale has been assumed to be consistent with unity, and these uncertainties are added in quadrature to determine a length scale systematic uncertainty of 0.3% on the product $\Sigma_x\Sigma_y$ and hence the relative uncertainty on the determination of σ_{vis}.

	Horizontal	Vertical
Beam 1 Length Scale	-1.0010 ± 0.0004	$+0.9955 \pm 0.0003$
Beam 2 Length Scale	-0.9981 ± 0.0003	$+0.9983 \pm 0.0003$
Beam Separation Scale	-0.9996 ± 0.0003	$+0.9969 \pm 0.0002$

Table 7: Length scale calibrations at the ATLAS interaction point. Values shown are the ratio of the beam displacement measured by ATLAS using the primary vertex position to the nominal displacement entered into the accelerator control system. Ratios are shown for each individual beam in both planes, but also for the beam separation length scale, which is the value that determines the convolved beam size in the *vdM* scan. The negative value for the horizontal calibration reflects the difference between the ATLAS and LHC coordinate systems. Errors shown are statistical only from the linear fits.

5 Calibration Uncertainties

This section outlines the systematic uncertainties which have been evaluated for the measurement of σ_{vis} from the *vdM* calibration scans. Table 8 summarizes the results.

Bunch charge product

The determination of this uncertainty has been described in Section 3.

Beam centering

If the beams are not perfectly centered in the non-scanning plane at the start of a *vdM* scan, the assumption that the luminosity observed at the peak is equal to the maximum head-on luminosity

[1]The length scale calibration performed in October 2010 is not applicable due to the different $\beta^\star$ configuration.

is not correct. The beams were centered at the beginning of the scan session, and the maximum observed non-reproducibility in relative beam position at the peak of the scan was $3\,\mu$m, corresponding to a 0.1% error on the peak instantaneous interaction rate.

Emittance growth

The *vdM* scan formalism assumes that the luminosity and the convolved beam sizes $\Sigma_{x/y}$ are constants, or more precisely that the transverse emittances of the two beams do not vary significantly either in the interval between the horizontal and the associated vertical scan, nor within a single x or y scan.

Emittance growth between scans would manifest itself by a slight increase, from one scan to the next, of the measured value of Σ, and by the simultaneous decrease of the peak specific luminosity (*i.e.* of the specific visible interaction rate at zero beam separation). Both effects are clearly visible in the May scan data shown in Section 2, where Figure 5 shows the increase in Σ and Figure 6 shows the reduction in the peak interaction rate.

The emittance growth rate extracted from these measurements is approximately constant from one scan to the next during fill 1783.

In principle, when computing the visible cross-section using Equation 4, the increase in Σ from scan to scan should exactly cancel the decrease in specific interaction rate. In practice, the cancellation is almost complete: the bunch-averaged visible cross-sections measured in scan VII and VIII, using the LUCID algorithms (Tables 2, 3) or the BCM algorithms (Tables 4, 5), differ by at most 0.4% between these two scans. This is comparable to the 0.5% uncertainty due to emittance growth evaluated for scans IV-V in October 2010.

Emittance growth within a scan would manifest itself by a very slight distortion of the scan curve. The associated systematic uncertainty determined by toy Monte Carlo with the observed level of emittance growth was found to be negligible.

Beam-position jitter

At each step of a scan, the actual beam separation may be affected by random deviations of the beam positions from their nominal setting. The magnitude of this potential "jitter" has been evaluated from the shifts in relative beam centering recorded during the length-scale calibration scans described in Section 4, and amounts to 0.6 μm RMS. The resulting systematic uncertainty on $\sigma_{\rm vis}$ is obtained from randomly displacing each measurement point in a simulated scan by this amount, and taking the RMS of the resulting variations in fitted visible cross-section. This procedure yields a $\pm 0.3\%$ systematic error associated with beam-positioning jitter during scans VII and VIII.

$\sigma_{\rm vis}$ consistency

The calibrated $\sigma_{\rm vis}$ value found for a given detector and algorithm should be a universal scale factor independent of machine conditions or BCID. Comparing the $\sigma_{\rm vis}$ values determined by BCID in Figures 2 and 3, however, it is clear that there is some degree of correlation between these values and the scatter observed is not entirely statistical in nature. The RMS variation of $\sigma_{\rm vis}$ for each of the LUCID and BCM algorithms is consistently around 0.4%, except for the BCM_EventAND algorithms, which have much larger statistical uncertainties. An additional uncertainty of $\pm 0.4\%$ has been applied to account for this BCID dependence.

Length scale calibration

The length scale of each scan step enters directly into the extraction of $\Sigma_{x/y}$ and hence directly affects the predicted peak luminosity during a *vdM* scan. The length scale calibration procedure is described in Section 4 and results in a $\pm 0.3\%$ uncertainty for scans VII-VIII.

Absolute length scale of the ATLAS Inner Detector

The determination of the length scale relies on comparing the scan step requested by the LHC with the actual transverse displacement of the luminous centroid measured by ATLAS. This measurement relies on the length scale of the ATLAS Inner Detector (ID) tracking system (primarily the pixel detector) being correct in measuring displacements of vertex positions away from the center of the detector. An uncertainty on this absolute length scale was evaluated by analysing Monte Carlo events simulated using several different misaligned Inner Detector geometries. These geometries represent distortions of the ID which are at the extreme limits of those allowed by the data-driven ID alignment procedure. Samples were produced with displaced interaction points to simulate the transverse beam displacements seen in a *vdM* scan. The variations between the true and reconstructed vertex positions in these samples give a conservative upper bound of ±0.3% on the uncertainty on the determination of σ_{vis} due to the absolute ATLAS ID length scale.

Fit model

The *vdM* scan data are analysed using a fit to a single Gaussian plus a constant background term. Refitting the data with several different models including a cubic spline and no constant term leads to different values of σ_{vis}. The most significant difference for the current reference algorithm (BCMH_EventOR) occurs when the constant term, normally subtracted before determining $\mu_{\text{vis}}^{\text{MAX}}$ and Σ, is assumed to be part of the luminosity curve by integrating the Gaussian plus constant term out to the scan range of $\pm 6\sigma_{\text{b}}$. Taking this maximum deviation as a measure of the systematic uncertainty due to the fit model results in an error of ±0.8%.

Transverse correlations

In the presence of linear *x*-*y* coupling in either beam, and provided the horizontal and vertical emittances are sufficiently different, the luminosity distribution as a function of the beam separation in the *x*-*y* plane may transform from an upright ellipse into a tilted ellipse, potentially resulting in a slight underestimation of Σ_x or Σ_y [8]. The analysis of the measured transverse displacements of the luminous region during the scans from reconstructed event vertex data provides a 0.1% upper limit on the associated systematic uncertainty. This is comparable to the upper limit derived, during 2010 LHC running, from direct measurements of the LHC lattice functions by resonant excitation combined with emittance ratios based on wire-scanner data [9].

In previous *vdM* scans, the luminosity profiles were best fit by a one-dimensional double-Gaussian distribution (in either x or y). For a generalized two-dimensional distribution this can lead to non-linear correlation terms such as $(\tilde{\Sigma}_x\tilde{\Sigma}_y)^{-1} = f/(\sigma_{1,x}\sigma_{1,y}) + (1-f)/(\sigma_{2,x}\sigma_{2,y})$, where the indices 1, 2 denote the first and second two-dimensional Gaussian functions, and f is the fraction of the core Gaussian in the Gaussian sum. Here the horizontal and vertical planes do not factorize, as in the single Gaussian case.

The possible impact of this effect was studied using LUCID_EventOR data (which has the highest statistics per scan point) and employing a generalized double-Gaussian fit simultaneously to the x and y scan data under various assumptions. The largest effect observed was 0.5% and this has been adopted as the systematic uncertainty due to any possible non-linear correlations. This is smaller than the ±0.9% uncertainty applied to the October 2010 scan due to the greatly reduced second Gaussian component observed in the May 2011 scan.

μ dependence

Scans VII-VIII were taken over a range $0 < \mu < 2.6$ so uncertainties on the μ correction can directly affect the evaluation of σ_{vis}. Figure 8 shows the variation in measured luminosity as a

function of μ between several algorithms and detectors, and on the basis of this agreement an uncertainty of ±0.5% has been applied for scans VII-VIII.

BCM consistency

The *vdM* scan procedure calibrates a particular luminosity algorithm at a single point in time under conditions which are rather different from normal physics data taking. As discussed more fully in Section 8, the agreement between the luminosity observed by the various algorithms is an important test of the stability of the calibration over long time periods and under differing beam conditions, including higher μ values and shorter bunch spacing.

The luminosity reported by the BCMV algorithms during routine physics fills differs from that of the BCMH algorithms by about 0.7% in spite of an excellent agreement during the *vdM* scans themselves (see for instance Figure 8). While there is some evidence that this is due to an instrumental effect in the BCMV device during the scans, it cannot be excluded that this represents some unknown uncertainty in the *vdM* calibration. A systematic uncertainty of ±0.7% has been conservatively applied to cover this effect.

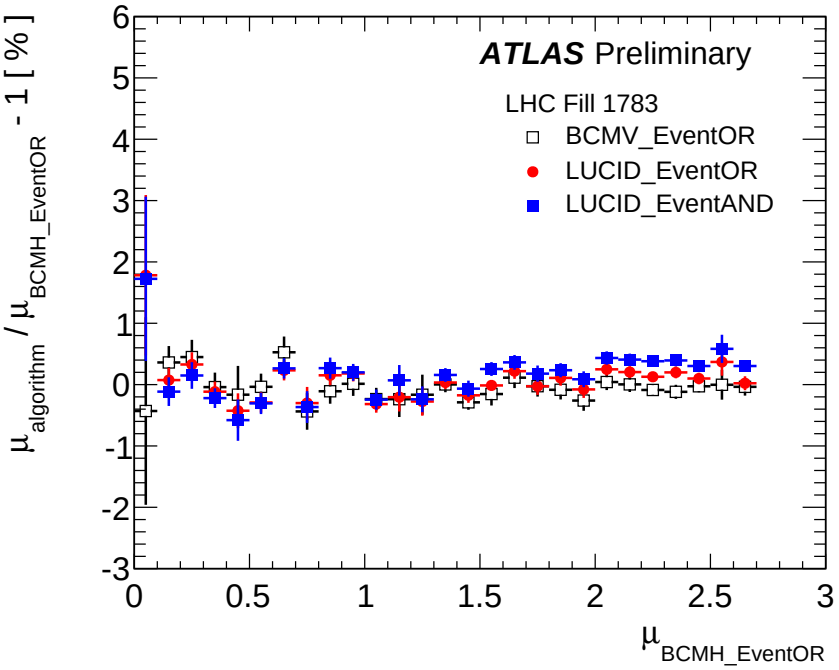

Figure 8: Fractional deviation in the average value of μ obtained using different algorithms with respect to the BCMH_EventOR value as a function of μ during Scans VII-VIII.

6 Calibration Results

The average of the σ_{vis} values found in the two May 2011 scans is used to provide the best estimate of the visible cross-section $\overline{\sigma}_{\text{vis}}$ for each luminosity method as shown in Table 9. This table also indicates the systematic uncertainties on the determination of $\overline{\sigma}_{\text{vis}}$ as discussed in Section 5. All systematic uncertainties have been assumed to be fully correlated between the two scans, and common to all detectors and algorithms. The results of the 2010 calibration are also shown for comparison.

Source	Relative Uncertainty
Bunch charge product	3.0%
Beam centering	0.1%
Emittance growth	
and other non-reproducibility	0.4%
Beam-position jitter	0.3%
Bunch-to-bunch σ_{vis} consistency	0.4%
Length scale calibration	0.3%
Absolute ID length scale	0.3%
Fit model	0.8%
Transverse correlations	0.5%
μ dependence	0.5%
BCM consistency	0.7%
Total	3.4%

Table 8: Relative systematic uncertainties on the determination of the visible cross-section σ_{vis}.

The differences in $\overline{\sigma}_{\text{vis}}$ values between the 2010 and 2011 scans are due in part to hardware changes in both the BCM and LUCID detector readout which occurred over the 2010-11 winter shutdown and early in the 2011 data taking. This point is discussed further in Section 8.

	2011 $\overline{\sigma}_{\text{vis}}$ (mb)	2010 $\overline{\sigma}_{\text{vis}}$ (mb)
LUCID_EventAND	13.44 ± 0.00 ± 0.46	13.04 ± 0.01 ± 0.44
LUCID_EventOR	42.51 ± 0.01 ± 1.45	41.67 ± 0.02 ± 1.40
LUCID_EventA	27.95 ± 0.01 ± 0.95	
LUCID_EventC	28.01 ± 0.01 ± 0.95	
BCMH_EventAND	0.1359 ± 0.0002 ± 0.0046	0.1316 ± 0.0005 ± 0.0045
BCMV_EventAND	0.1387 ± 0.0002 ± 0.0047	
BCMH_EventOR	4.689 ± 0.002 ± 0.159	4.594 ± 0.005 ± 0.147
BCMV_EventOR	4.736 ± 0.002 ± 0.161	

Table 9: Best estimate of the visible cross-section determined from *vdM* scan data for 2011 and 2010. Errors shown are the statistical component and the total systematic uncertainty.

7 Calorimeter Luminosity Measurements

In order to provide a cross-check of the stability and μ-dependence of the LUCID and BCM algorithms, an independent measure of the luminosity has been developed using the ATLAS calorimeters. In the first method, the PMT current drawn in Tile Calorimeter (TileCal) modules is used, while in the second the current drawn across the liquid argon gaps in the Forward Calorimeter (FCal) modules is used. Since the currents drawn are related to the mean number of particles interacting in each calorimeter, the observed currents are sensitive to the luminosity.

7.1 Tile Luminosity Measurement

The Tile Calorimeter is the central hadronic calorimeter of ATLAS. It is a sampling calorimeter constructed from iron plates (absorber) and plastic tile scintillators (active material). TileCal is located

between the Liquid Argon electromagnetic calorimeter and the muon system and covers the pseudorapidity range $|\eta| < 1.7$. The detector consists of three cylinders, a central long barrel (LB) and two smaller extended barrels (EB), one on each side of the long barrel. Each cylinder is divided into 64 slices in ϕ (modules) and segmented into three radial sampling layers. Cells are then defined in each layer according to a projective geometry.

Each cell is connected by optical fibers to two photomultiplier tubes, and the signal from each PMT is divided into three outputs. The first output is connected to the main digital readout chain, while the second output provides data for the L1Calo trigger. The third output goes to an integrator system that integrates the anode current of each PMT with a time constant of 10 ms over a range of currents from 0.1 nA to 1.2 mA.

The PMT current readout has been primarily designed to calibrate the response of the individual cells using a radioactive ^{137}Cs source. During collisions, however, the measurement of the anode current provides a luminosity-dependent signal, since the energy deposited in any TileCal cell is proportional to the total pp interaction rate. The proportionality constant, which must be calibrated, depends on the layer, the size of the cell and its η position. The luminosity during a *vdM* scan is too low to perform an absolute calibration of the TileCal response, so a relative calibration has been made comparing the TileCal currents to the LUCID_EventOR algorithm for a single ATLAS run (166786) recorded on 13 October 2010.

There are two different methods used to calibrate the TileCal current response. The first method consists of calibrating the average current for a selected set of good cells, while the second calibrates each cell individually. Figure 9 shows the calibration of the average response of the cells at $|\eta| \approx 1.25$ in the innermost radial layer to the LUCID_EventOR luminosity for a single ATLAS run in 2010. This particular set of cells was chosen as it observes the highest currents as a function of luminosity of any TileCal module. This calibration method has the advantage over single-cell calibrations of using exactly the same set of cells to measure the luminosity over a range of time, resulting in reduced systematic uncertainties and residual variations. In order to validate the calibration procedure, the TileCal luminosity measurement was compared to LUCID_EventOR for all of the 2010 pp data where the luminosity was greater than 35×10^{30} cm^{-2} s^{-1}. The RMS residual deviation between Tile and LUCID was found to be about 0.2% when comparing the average luminosity measured over a time range of about 2 minutes.

At the higher luminosities encountered in 2011, TileCal started to suffer from frequent trips in the low voltage power supplies causing the intermittent loss of current measurements from several modules. For this data, the second method based on the calibration of individual cells is applied, which has the advantage of allowing different sets of cells to be used based upon the availability of TileCal current data. Since these sets of cells can vary significantly over time, this method is more sensitive to the residual variations of the cell calibration constants. For the 2011 data, the RMS variation of the TileCal luminosity measurement is estimated to be about 0.5% based on the agreement between individual cells and the typical number of calibrated cells available to make a measurement.

7.2 FCal Luminosity Measurement

The FCal is a sampling calorimeter that covers the pseudorapidity range $3.2 < |\eta| < 4.9$ and is housed in the two end-cap cryostats along with the electromagnetic end-cap (EMEC) and the hadronic end-cap (HEC) calorimeters. Each of the two FCal modules (FCal A and FCal C) is divided into three longitudinal absorber matrices, one made of copper (FCal-1) and the other two of tungsten (FCal-2/3). Each matrix contains tubes arranged parallel to the beam axis filled with liquid argon as the active medium. An FCal tube houses a central rod on which a high-voltage (HV) is applied to drift ionization electrons by an effective electric field of approximately 1 kV/mm. Each FCal-1 matrix is divided into 16 ϕ-sectors, each of them fed by four independent high-voltage (HV) lines. The primary function of the high-voltage system is to provide the calorimeter liquid argon gaps with a stable electric field. The

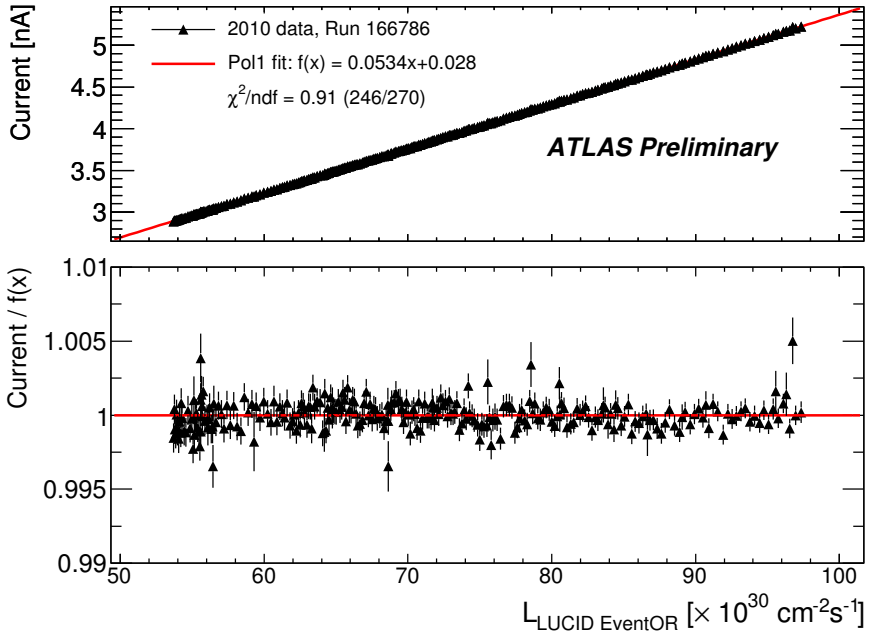

Figure 9: Calibration of TileCal PMT currents to LUCID_EventOR luminosity for a single ATLAS run in 2010.

regulation is performed by injecting a current to compensate for the ionization created by high energy charged particles passing through the liquid argon. As the particle flux intensity is directly proportional to the pp interaction rate, the current injected by the FCal-1 high-voltage system to compensate for ionization losses is directly proportional to the luminosity. All of the 128 FCal-1 high-voltage lines can be individually calibrated.

Similar to TileCal, the FCal luminosity measurement cannot be directly calibrated during a *vdM* scan because the total luminosity is below the sensitivity of the FCal technique. Instead, calibrations were evaluated for each usable HV line independently by comparing to the LUCID_EventOR luminosity for the same ATLAS run used by TileCal described above. In order to check the validity of the calibration throughout the 2010 data taking period, the calibrated FCal luminosity based on a single run was compared to the LUCID_EventOR luminosities for a set of runs recorded during October 2010 when the luminosity was high enough for the FCal technique to work. The distribution of $\mathcal{L}_{\mathrm{LUCID}}/\mathcal{L}_{\mathrm{FCal}}$ computed approximately every two minutes, independently for each high-voltage line, is shown in Figure 10. A residual variation of 0.5% is observed.

7.3 Comparison of TileCal and FCal

While both Tile and FCal showed good agreement with the LUCID_EventOR luminosity measurement in 2010, direct comparisons of the Tile and FCal values in 2011 show a difference of around 2%. Figure 11 shows the relative difference between the TileCal and FCal luminosity measurements for a range of data in 2011. An overall offset of $\approx 2\%$ is clearly visible, as well as evidence of a shift of calibration during 2011 of order 0.7% leading to the double-peaked distribution.

To compensate for unknown changes in the calorimeter current dependence on luminosity over the 2010-11 winter shutdown, an *ad hoc* rescaling of the luminosity for both calorimeter methods has been applied based on the integrated luminosity estimate compared to BCMH_EventOR. The rescaling was

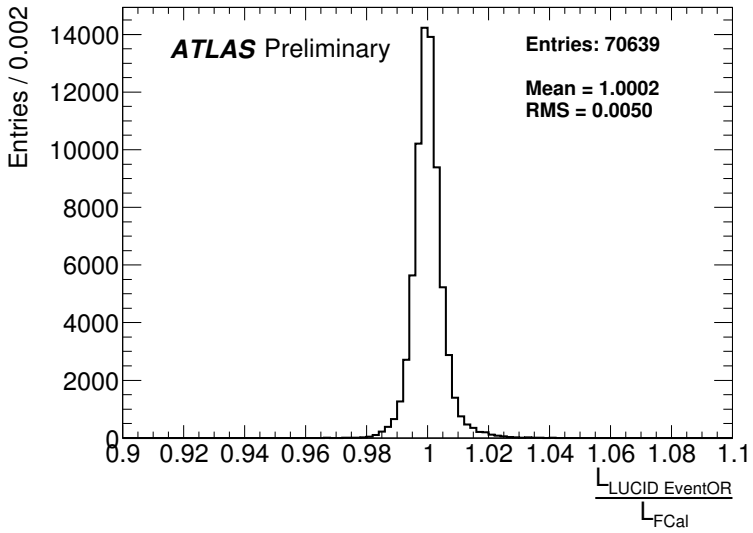

Figure 10: Distribution of the ratio $\mathcal{L}_{\mathrm{LUCID}}/\mathcal{L}_{\mathrm{FCal}}$ for 17 ATLAS runs in 2010. One ratio is computed approximately every two minutes for each high-voltage line.

performed using ATLAS run 182161, recorded on 18 May 2011, which is one of the first runs recorded after the 15 May 2011 *vdM* scan. A correction factor of 0.9884 is determined for the TileCal luminosity estimate compared to the 2010 calibration, while for FCal a correction factor of 1.0091 is determined. Based on this rescaling, the calorimeter methods still provide an independent check of the long-term stability of the various luminosity algorithms, as well as an overall test of the μ dependence. These comparisons will be presented in Section 8.

8 Long-term Stability and Consistency

The $\overline{\sigma}_{\mathrm{vis}}$ values determined in Section 6 allow each calibrated algorithm to provide luminosity measurements over the course of the 2011 run. For producing the integrated luminosity value used in ATLAS physics results, the BCMH_EventOR algorithm has primarily been used, with the LUCID_EventOR algorithm being used during periods when BCM data were unavailable.

The calibration of $\overline{\sigma}_{\mathrm{vis}}$, however, is made only at one point in time and at a relatively low value of μ compared to the range of μ values routinely seen in 2011 operations so far ($0 < \mu < 14$). Several additional effects due to the LHC operating conditions with a large number of bunches and large μ values must be considered, and additional uncertainties related to the extrapolation of the *vdM* scan calibration to the complete 2011 data sample must be evaluated.

Several specific corrections are described below, along with more general uncertainties related to the agreement and stability of the various methods available to determine the luminosity over the 2011 run.

8.1 Hardware Changes

Several changes were made to the readout chain of both the BCM and LUCID detectors before and during the early 2011 data taking period.

During the 2010-11 winter shutdown, resistors on the BCM front-end boards were replaced to increase the dynamic range of the low-gain BCM signal used for beam aborts. While the adjustments were performed in a way that should have left the high-gain BCM signal (used for the luminosity measurement) unchanged, variations at the percent level remain possible. As a result, the BCM calibration in

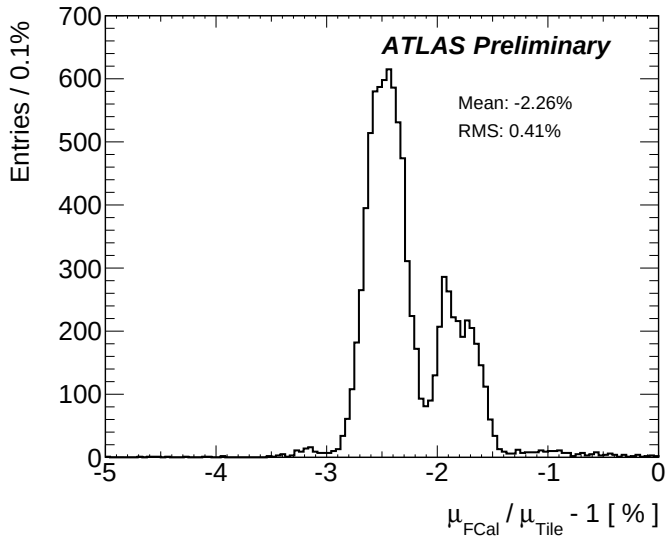

Figure 11: Distribution of the ratio of the TileCal and FCal luminosity measurements for 20 ATLAS runs in 2011. Each entry represents approximately one minute of data.

2010 is not expected to be directly applicable to the 2011 data.

On 21 April 2011, the BCM thresholds were adjusted to place the thresholds at a more optimal point in the detector response plateau. As this change was made during a period with stable beams, the ratio of the BCM luminosity to that of any other detector shows a clear step, which can be used to measure directly the relative change in σ_{vis} due to this adjustment. After the threshold change, the luminosity measured by BCMH_EventOR was observed to increase with respect to other detectors by +3.1%, which implies that the σ_{vis} value for BCMH_EventOR actually increased by this amount. For BCMV the equivalent figure is +4.1%. Since the 2011 *vdM* scan calibration happened after this date, for any BCM data taken before this threshold change, the σ_{vis} value applied has been scaled down accordingly from the 2011 calibrated value. The total change in σ_{vis} for BCMH_EventOR shown in Table 9 is +2.1%, implying that over the 2010-11 winter shutdown the BCMH_EventOR response changed by about −1%.

During the LHC technical stop in early April 2011, the LUCID receiver cards were changed to improve the performance of the readout with 50 ns bunch spacing. Since this change was made during a period with no collisions, there is no direct measurement of the shift in LUCID calibration. Using data taken before and after the technical stop it can be estimated that the LUCID_EventOR σ_{vis} value increased by about 2–3%. The total change in LUCID_EventOR calibration from 2010 to 2011 shown in Table 9 is +2.0%, which indicates that the LUCID σ_{vis} calibration is consistent between 2010 and 2011 at a level of approximately 1%.

8.2 Afterglow Subtraction

Both the LUCID and BCM detectors observe some small activity in the BCIDs immediately following a collision [2]. This "afterglow" is most likely caused by photons from nuclear de-excitation, which in turn is induced by the hadronic cascades initiated by pp collision products. With a 2011 bunch spacing of 50 ns and a relatively large number of bunches injected into the LHC, this afterglow tends to reach a fairly stable equilibrium after the first few bunches in a train, and is observed to scale with the instantaneous luminosity.

Figure 12 shows the luminosity reported by LUCID_EventOR and BCMH_EventOR for a span of 800 BCIDs within a fill in June 2011 with 1042 colliding bunch pairs. The afterglow level can be seen

to be roughly constant at the 1% level for LUCID_EventOR and at the 0.5% level for BCMH_EventOR during the bunch train, and dropping during gaps in the fill pattern.

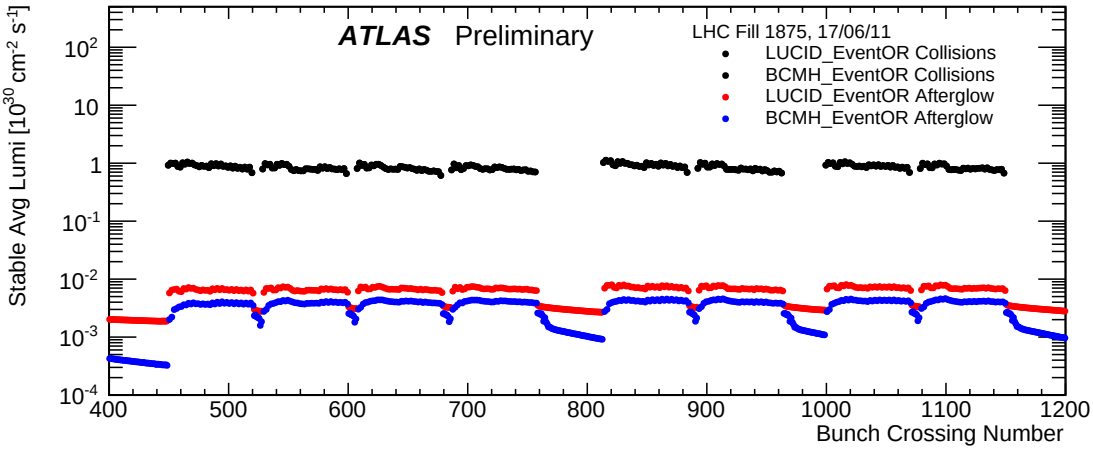

Figure 12: Observed luminosity averaged over the fill as a function of BCID for the LUCID_EventOR and BCMH_EventOR algorithms for a single LHC fill with 1042 colliding bunch pairs. On this scale the BCMH and LUCID luminosity values for colliding BCIDs are indistinguishable. The small "afterglow" luminosity comes in BCIDs where no bunches are colliding and are the result of induced activity seen in the detectors. Only 800 BCIDs are shown so that the details of the afterglow in the short and long gaps in the fill pattern can be seen more clearly.

To assess the effect of afterglow, the probability of an afterglow event must be combined with the Poisson probabilities outlined in Section 2.2 to assess the correction to the observed μ value. For EventOR algorithms, this correction works out to be the simple correction $\mu = \mu_{\text{obs}} - \mu_{\text{bgd}}$ while for the EventAND algorithms a considerably more involved formula must be applied. To estimate μ_{bgd}, the calibrated μ value observed in the BCID immediately preceding a collision has been used. Different estimates using the following BCID or the average of the preceding and following BCIDs produce negligibly different results.

This afterglow correction has been applied to all BCM and LUCID luminosity determinations except for the BCM_EventAND algorithm, which observes a negligible level of afterglow. Since the afterglow level in the BCID immediately following a colliding bunch may be higher than in the second BCID after a colliding bunch, BCIDs at the end of a bunch train have been used to evaluate the possible overestimate of the afterglow correction. Based on these comparisons, a systematic uncertainty of 0.2% has been evaluated for the BCM_EventOR algorithms which are being used to provide the absolute physics luminosity scale.

8.3 LUCID μ Correction

When constructing the exponential formulae in Section 2.2, a basic assumption is that the probability of not selecting a bunch crossing with n interactions $P_0(n)$ can be calculated from the probability of not selecting a bunch crossing with one interaction $P_0(1)$ according to $P_0(n) = [P_0(1)]^n$. As described in Reference [2], Monte Carlo studies of the LUCID detector have shown that this assumption is not always completely correct due to so-called "migration", an effect where multiple interactions, which are individually below threshold, add together to create an event which is above threshold.

Another way of constructing a formula to calculate μ from the observed event rate is to pile up (overlay) events corresponding to exactly one interaction and determine the rate at which these events

pass the event selection criteria as a function of μ. Such event samples can be obtained either from Monte Carlo simulations or by manipulating real data samples recorded at very low luminosity with a random trigger.

Using data taken in special low-luminosity runs with $\mu \approx 0.01$, a pile-up sample has been constructed from real data. A randomly triggered sample of low-μ events has the wrong proportion of events with zero interactions (ZERO events), so as a first step events where all Lucid Cerenkov tubes have signals in the region consistent with no photons are removed at random until the number of AND, OR, and ZERO events corresponds to what is expected in a sample with exactly one interaction assuming the measured σ_{vis} values are correct.

The sample of events with one interaction is then piled up to create samples of 2, 3, 4.....30 interactions by adding up the signals measured by the FADCs from each Cerenkov tube. Cuts corresponding to the trigger thresholds are applied to the FADC signals in each sample and the probability of getting a trigger is recorded as a function of the number of interactions. These probabilities for a fixed number of interactions are used to calculate μ by assuming the number of interactions to be Poisson distributed.

A comparison between the μ-values calculated with the pile-up method to that from the exponential formulae is shown in Figure 13. The multiple interactions which are individually below threshold for selecting an event tend to cause the exponential formulae to overestimate the luminosity at high values of μ. For LUCID_EventOR, the difference can be described by a linear function that gives a 1% correction at μ=10 . The LUCID_EventAND comparison shows a correction of slightly more than 2% at μ = 10.

These pile-up corrections have been applied to all LUCID data used to evaluate luminosity during physics operations and in the comparison plots shown in Figures 14–16. For simplicity, these corrections have not been applied to the LUCID data during the low-μ *vdM* scans where the effect would be small, and within the quoted uncertainty of ±0.5% for μ-dependence during the scan.

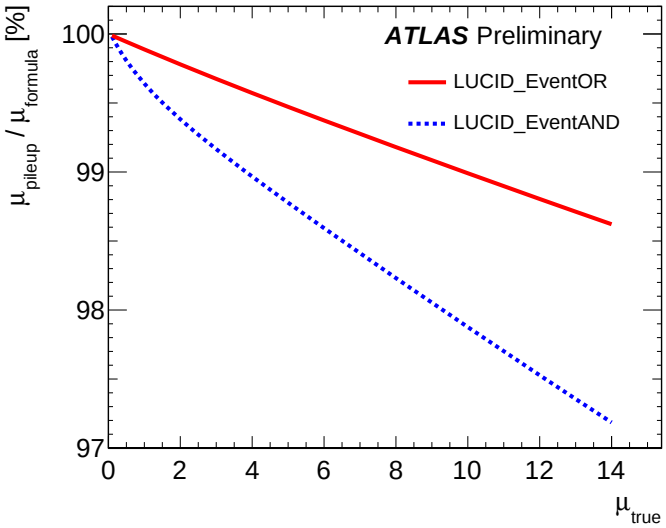

Figure 13: Ratio of the luminosity determined by the pile-up method to the exponential formulae described in Section 2.2 as a function of μ for the LUCID_EventOR and LUCID_EventAND algorithms.

8.4 LUCID PMT Current Correction

Due to the increase in the total luminosity delivered by the LHC, both in terms of the number of bunches colliding and of the average μ per bunch, the LUCID PMTs are now operating in a regime where the average anodic PMT current is of order 10μA which has an observable effect on the PMT gain.

Uncorrected, this effect shows up both as an apparent μ dependence of the luminosity, since the PMT currents are highly correlated with the average μ during a fill, as well as a long-term time dependence in the LUCID luminosity value, since the number of colliding bunches has steadily increased in 2011. The magnitude of this effect is of order 2% on the LUCID luminosity.

The total anodic current summed over all LUCID tubes, normalized to the number of collision BCIDs in a given fill, has been observed to produce a linear deviation of the LUCID_EventOR luminosity with respect to the BCMH_EventOR value. A correction for this effect has been evaluated using a single ATLAS run with 1042 colliding bunches to remove the linear dependence of the LUCID luminosity on anodic PMT current.

The effect of the correction can be seen in Figure 14, where the difference between μ measured by LUCID_EventOR and BCMH_EventOR is shown as a function of time, both before (above) and after (below) the PMT-current correction. The different colors refer to different ranges of the measured μ. Only three μ ranges have been shown for clarity in the Figure, but all μ ranges show a similar effect. For each time interval, the difference between the two algorithms is independent of μ, reflecting a negligible relative μ-dependence between the two algorithms. However, while before any PMT-current correction is applied a clear dependence can be seen as a function of time (and thus of the current drawn by the PMTs), after the correction such a dependence is no longer present.

This PMT current correction has been applied to all LUCID data used to describe luminosity during physics operations. As a result, the LUCID values shown in Figures 15 and 16 are implicitly tied to the BCMH luminosity scale at one point in time, although any long-term variation observed is still significant. Similarly, any linear μ dependence between the LUCID and BCMH response, which is uniform over all runs, will be removed by this correction factor. Higher-order variations, however, will still be visible.

8.5 Long-term Stability

One key source of potential uncertainty is the assumption that the $\overline{\sigma}_{\text{vis}}$ calibration determined in a set of *vdM* scans is stable across the entire 2011 data set. Several effects could degrade the long-term stability of a given detector, including slow drifts in the detector response and sensitivity to varying LHC beam conditions, particularly the total number of colliding bunches.

Because the number of colliding bunches increased more or less monotonically during the 2011 data taking period, it is not possible to disentangle these two effects, so the tests of long-term stability should be viewed as covering both possibilities.

Figure 15 shows the ratio of integrated luminosity per ATLAS run as measured by a variety of luminosity algorithms, compared to the reference algorithm BCMH_EventOR, over a range of 2 ½ months. As discussed in Section 7, the absolute TileCal and FCal luminosity values based on 2010 calibrations have been rescaled to provide a relative measurement of stability for 2011.

While there is a significant scatter amongst the calorimeter results shown in Figure 15, there is no evidence for any long-term variation and the peak-to-peak deviation for both is within ±1%. The ratio of BCMV_EventOR to BCMH_EventOR agrees very well, except for the 0.7% offset discussed in Section 5. Since these are fundamentally the same detector (although not specifically the same readout) the stability here tests only the internal consistency of the BCM. Finally, the ratio of LUCID_EventOR to BCMH_EventOR shows a peak-to-peak variation of ±1%, which may reflect a remaining dependence of the LUCID response on the number of colliding bunches, or an incomplete correction for the PMT current dependence.

A systematic uncertainty on long-term stability, which includes any effects related to dependence on the number of colliding bunches or other operational conditions seen in the 2011 data, is conservatively set at ±1%.

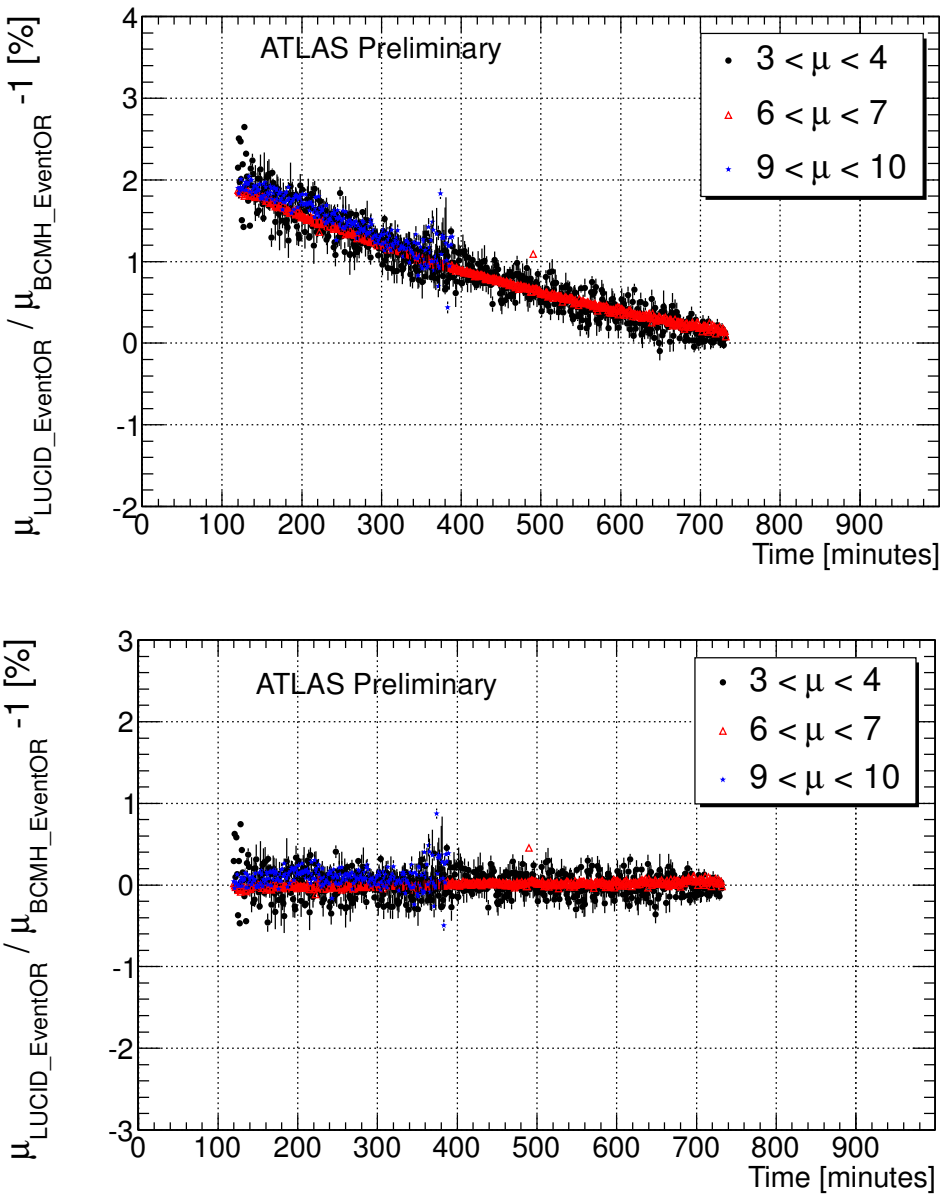

Figure 14: Ratio of LUCID_EventOR to BCMH_EventOR as a function of time before any PMT-current correction (top) and after the PMT-current correction (bottom). The various colors refer to different ranges of μ (see text for explanation).

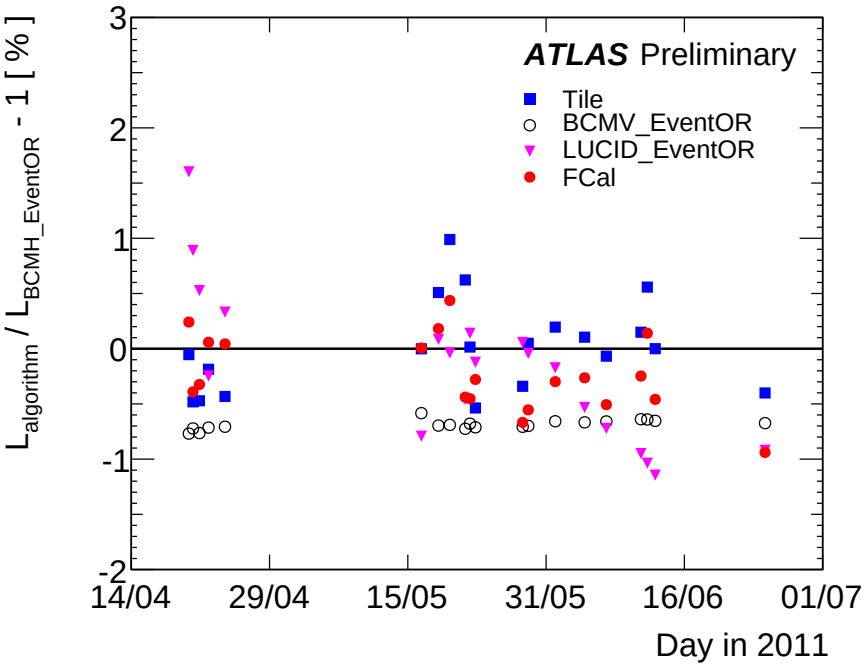

Figure 15: Fractional deviation in the integrated luminosity obtained using different algorithms with respect to the BCMH_EventOR value as a function of time. Each point shows the average deviation for a single ATLAS run. Statistical uncertainties per point are negligible.

8.6 μ Dependence

A final cross-check is made on the luminosity ratio with respect to BCMH_EventOR as a function of the number of interactions per crossing. For BCID-dependent algorithms (LUCID and BCM) this comparison can be made on a bunch-by-bunch basis. For the calorimeter methods, however, this comparison can be made only on the number of interactions averaged over all BCIDs ($\langle\mu\rangle$) at a given point in time.

Figure 16 shows this comparison for several algorithms. The same scaling of the calorimeter data described in the previous section has been applied here. The calorimeter-based methods show a $\langle\mu\rangle$ dependence with respect to BCMH_EventOR, although the two calorimeter methods are not completely consistent with each other either. The BCMV and LUCID curves show considerably less $\langle\mu\rangle$ dependence with respect to BCMH_EventOR.

If the variation over the $\langle\mu\rangle$ range from 4 to 8 is considered, all methods agree to within $\pm 1\%$. The more relevant consideration is the possible deviation of the average luminosity scale at $\langle\mu\rangle \approx 6$ when extrapolated from the low μ range where the *vdM* calibration is performed. In this comparison, the observed slope between Tile and BCMH_EventOR would indicate about a 1% offset, with the FCal data indicating a value which is somewhat larger. Again, because of the PMT current correction, any linear dependence between the LUCID and BCMH data would not be observed in this plot, although an alternative analysis performed on individual BCIDs averaged over the duration of a fill (to take out the time-dependent PMT shifts without an explicit correction) agrees very well between BCMH and LUCID.

As a result of all the information available, a systematic uncertainty of $\pm 1\%$ has been applied to account for any possible μ dependence in the extrapolation from the low μ *vdM* scan calibration to the higher μ physics data.

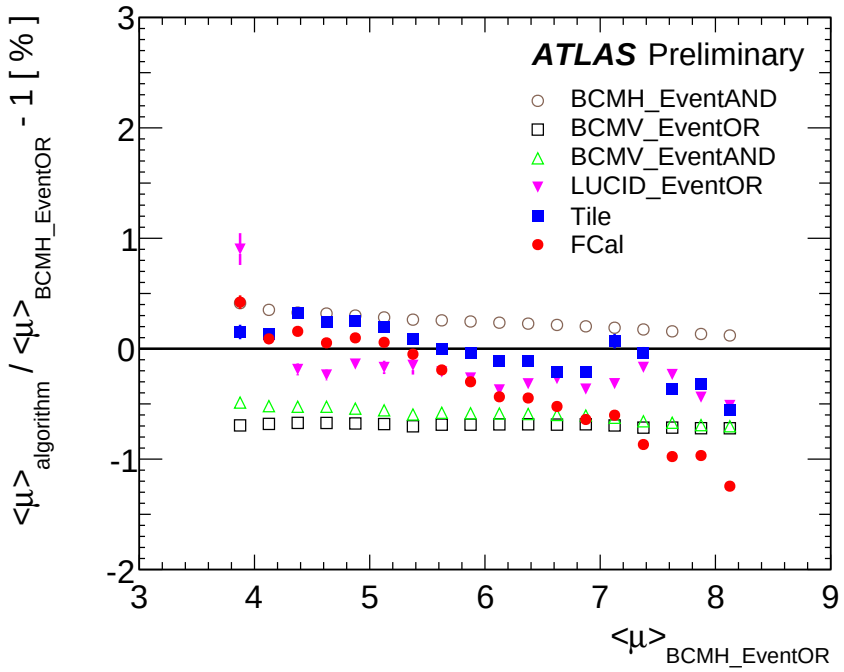

Figure 16: Fractional deviation in the average number of interactions per bunch crossing $\langle\mu\rangle$ (averaged over BCIDs) obtained using different algorithms with respect to the BCMH_EventOR value as a function of $\langle\mu\rangle$. Statistical uncertainties per point are negligible.

8.7 Total Luminosity Uncertainty

Table 10 lists the contributions to the total systematic uncertainty on the luminosity scale provided for physics analyses in the 2011 data sample. A total relative uncertainty of 3.7% is found.

Uncertainty Source	$\delta\mathcal{L}/\mathcal{L}$
vdM Scan Calibration	3.4%
Afterglow Correction	0.2%
Long-term consistency	1.0%
μ Dependence	1.0%
Total	3.7%

Table 10: Relative uncertainty on the calibrated luminosity scale broken down by source.

9 Conclusions

The luminosity scale determined by the ATLAS collaboration for 2011 has been evaluated based on 2011 *vdM* scan data. Because of various operational issues with the LUCID detector described in Section 8, the BCMH_EventOR algorithm has been used as the reference algorithm for ATLAS physics results in 2011 pp operations at $\sqrt{s}$ = 7 TeV. The calibration of the BCMH_EventOR visible cross-section is determined to be σ_{vis} = 4.689 ± 0.159 mb where the uncertainty is dominated by the understanding of the bunch charge product during the *vdM* scan. The relative uncertainty on the luminosity scale applied to the 2011 pp data at $\sqrt{s}$ = 7 TeV, including the extrapolation of the *vdM* scan calibration to the entire

2011 data sample, is found to be ±3.7%.

References

[1] ATLAS Collaboration, G. Aad et al., *The ATLAS Experiment at the CERN Large Hadron Collider*, JINST **3** (2008) S08003.

[2] ATLAS Collaboration, G. Aad et al., *Luminosity Determination in pp Collisions at sqrt(s)=7 TeV Using the ATLAS Detector at the LHC*, Eur. Phys. J. **C71** (2011) 1630.

[3] ATLAS Collaboration, *Updated Luminosity Determination in pp Collisions at* $\sqrt{s} = 7$ *TeV using the ATLAS Detector*, ATLAS-CONF-2011-011, 2011.

[4] S. van der Meer, *Calibration of the effective beam height in the ISR*, CERN-ISR-PO-68-31, 1968.

[5] G. Anders et al., *LHC Bunch Current Normalisation for the October 2010 Luminosity Calibration Measurements*, CERN-ATS-Note-2011-016 PERF, in preparation.

[6] A. Jeff et al., *Design for a Longitudinal Density Monitor for the LHC*, MOPE055, Proc. International Particle Accelerator Conference (IPAC'10), Kyoto, Japan, 2010.

[7] ATLAS Collaboration, *Upper Limits on the Charge in Satellite Bunches for the October 2010 LHC Luminosity Calibration*, ATLAS-CONF-2011-049, 2011.

[8] Y. Cai, *Luminosity of asymmetric* e^+e^- *collider with coupling lattices*, SLAC-PUB-8479, 2000.

[9] S. M. White, *Determination of the absolute luminosity at the LHC*, CERN-THESIS-2010-139.